Hindawi
Advances in Civil Engineering
Volume 2019, Article ID 8658753, 16 pages
https://doi.org/10.1155/2019/8658753

Research Article

Dynamic Surface Subsidence Characteristics due to Super-Large Working Face in Fragile-Ecological Mining Areas: A Case Study in Shendong Coalfield, China

Chao Chen,[1] **Zhenqi Hu**,[2] **Jin Wang**,[3] **and Jitang Jia**[4]

[1]*College of Civil Engineering, Henan University of Engineering, Zhengzhou 451191, China*
[2]*School of Environment Science and Spatial Informatics, China University of Mining and Technology, Xuzhou 221116, China*
[3]*Beijing Key Laboratory of Traffic Engineering, Beijing University of Technology, Beijing 100124, China*
[4]*Institute of Land Reclamation and Ecological Restoration, China University of Mining and Technology (Beijing), Beijing 100083, China*

Correspondence should be addressed to Zhenqi Hu; huzq1963@163.com

Received 28 August 2018; Revised 19 November 2018; Accepted 12 December 2018; Published 22 January 2019

Guest Editor: Ray R. Zhang

The dynamic subsidence characteristics due to super-large working face (SLWF) are the basis for further understanding of land ecology damage in fragile-ecological mining areas. In order to acquire the evolution characteristics of dynamic subsidence parameters and surface cracks, a series of field monitoring and comparisons with previous studies were conducted. The results indicate that (1) the subsidence trough is characterized with self-healing characteristics, including rapid formation of subsidence trough, the convergence of deformation, a steep trough edge, the smaller range of surface cracks; (2) the dynamic curves of dynamic subsidence parameters conformed to the exponential function curve with an inflection point when the SLWF advanced ca. critical dimension, which is the commonality of the dynamic subsidence characteristics; and (3) the optimized monitoring strategy for land ecology damage is recommended, and more attention should be paid to the quantitative prediction of root damage due to coal mining. The research results would benefit mining damage control and civil engineering protection in fragile-ecological mining areas.

1. Introduction

Underground coal mining is one of the key drivers of land ecology damage worldwide in many countries, which poses a serious threat to the sustainable development of resources and energy [1–3]. China's coal production is among the highest productions in the world [4, 5]. As China's energy strategy moves westward, the Shendong Coalfield has become the major coal-producing area in China [6–8]. The favorable occurrences of coal resources are suitable for large-scale modern development [8–10]. Herein, the SLWF technology characterized with large panel dimension, large advancing speed, more safety, and high efficient (Figure 1) has been widely adopted in the Shendong Coalfield [6–11]. However, the ecological environment in the Shendong Coalfield is certainly fragile, and the highly intensive coal mining poses a great threat to the land ecology safety, which may cause further deterioration [6–8, 10]. Therefore, grasping the evolution characteristics and influencing factors of land ecology damage over mining process is essential to manage and mitigate the negative impacts of coal mining [1, 12]. Recently, land ecology damage due to underground coal mining, especially for the Shendong Coalfield, a representative fragile-ecological mining area, has gradually become an active research topic [7, 12–17]. Nevertheless, previous studies indicate that land ecology damage due to SLWF differs from that induced by traditional mining technologies, or in eastern China, and what really matters is

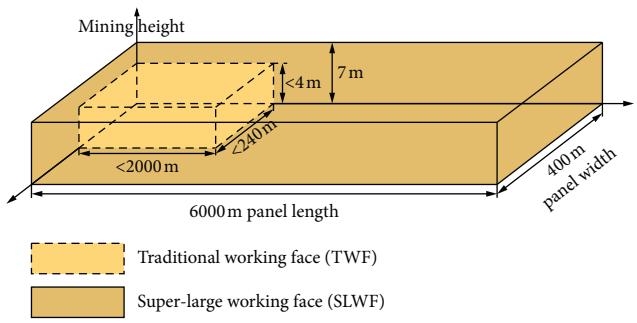

Figure 1: SLWF and TWF [10].

that land ecology damage commonly occurs in the dynamic mining subsidence process [14, 18, 19]. Furthermore, the magnitude of land ecology damage due to underground coal mining depends not only on the static subsidence parameters, but also on the evolution characteristics of dynamic subsidence parameters. Hence, adequate study on dynamic subsidence characteristics due to SLWF is the basis and precondition for further study on land ecology damage in fragile-ecological mining area [12, 14, 18].

However, the dynamic subsidence process is a relative complex spatiotemporal process influenced by various geological and mining factors. And the magnitude and form of surface movement and land damages varies in different coal fields [9, 20–22]. For instance, Salmi et al. [22] classified the subsidence process into two phases according to subsidence magnitudes. Additionally, dynamic subsidence is a well-known phenomenon and attracted the attentions of several researchers, performing large studies on dynamic subsidence characteristics due to coal mining, based on field monitoring in different coal fields of China [23–27], most of which are located in eastern China. Although some researchers conducted a series of studies on the surface movement and deformation [28–34], as well as mining-induced ground cracks in fragile-ecological mining area [35–37], for example, Yu et al. [35] studied the formation mechanism of the falling crack and proposed its control method, there are still areas lacking clarity and investigation. Particularly, there are some special subsidence characteristics, such as larger tangent values of angles of major influence, steep edges of subsidence troughs, etc, resulting from SLWF, and thick and unconsolidated aeolian sand with larger fluidity (lower mechanical strength). And the mechanical properties of aeolian sand are significantly different from those of the bedrock stratum. Moreover, the evolution characteristics of some dynamic subsidence parameters have not been well reported. And there is still a lack of analysis of evolutionary characteristics of surface cracks, which are essential for land ecology damage studies due to SLWF. Hence, based on the field data from the surface movement monitoring stations established above the SLWF, the evolution characteristics of dynamic subsidence parameters and surface cracks during the dynamic mining process have been acquired, and the impacts of mining and geological factors on the evolutionary characteristics were analyzed. Furthermore, some relevant scientific issues in the dynamic mining subsidence process were discussed, aiming to provide theoretical references for mining damage control and ecological restoration in the fragile-ecological mining areas.

2. Study Area

2.1. Physiographic Condition. The Shendong Coalfield (Figure 2), a typical fragile-ecological area mainly characterized by aeolian landform, is located in the transitional zones from the Mu us desert to the Loess Plateau [11, 15, 34], and the geographical position is from 38°52′–39°41′ north latitude, 109°51′–110°46′ east longitude, and covers an area of about 3800 km^2 with an altitude from 1000 to 1500 m above sea level, most of which covered by sand dune with a thickness varying between 20 and 50 m. Further, the geographical position of Daliuta colliery is from 39°13′–39°22′ north latitude, 110°12′–110°24′ east longitude. The topsoil comprises a high level of sandy soils characterized with a rough soil mechanical composition, poor capacity of water and nutrient preservation, and worsening wind erosion, which contributes to serious desertification. In addition, there is low vegetation coverage with sparse vegetation, and the main vegetations are herbage and artificial vegetation and other typical psammophilous vegetations [11, 15]. The coal field is characterized by a typical dry arid and semiarid plateau continental climate with less rain. The water resources are very precious, with average annual precipitation and evaporation of 413.5 mm and 2111.2 mm, respectively, and the meteorological elements are greatly influenced by the geographical environment [10].

2.2. Mining and Geological Conditions. This paper takes the 52305 SLWF of the Daliuta colliery as the study object, which is located in the third panel of the Daliuta colliery and excavation of the 5^{-2} coal seam commenced in September 2013 and completed in July, 2014. The adjacent old goaf of 52304 SLWF lied to the south of 52305 SLWF, and the virgin zone lied to the north. The thickness of the 5^{-2} coal seam ranges from 7.07 m to 7.7 m, and the dip angle varies between 1° and 3°, which is stable and belongs to flat seams. The 52305 SLWF is 280.5 m wide and 2881.3 m long, with an average mining height of 6.7 m. The overburden mainly comprises quaternary loose soils and bedrock, of which the average thicknesses are around 30 m and 138 m, respectively. And the average mining depth is ca. 230 m. The overlying surface exhibits a flat terrain covered by thick aeolian sand. The immediate roof and main roof of the extracted seam are siltstone and packsand, respectively. The main roof primarily comprises quartz, and the overlying rock is characterized with argillaceous cementation and current bedding. Additionally, the fully mechanized coal mining method and the fully caving method to manage the roof were employed in the SLWF. The practical excavation ratio was 93% when the mining was completed [37].

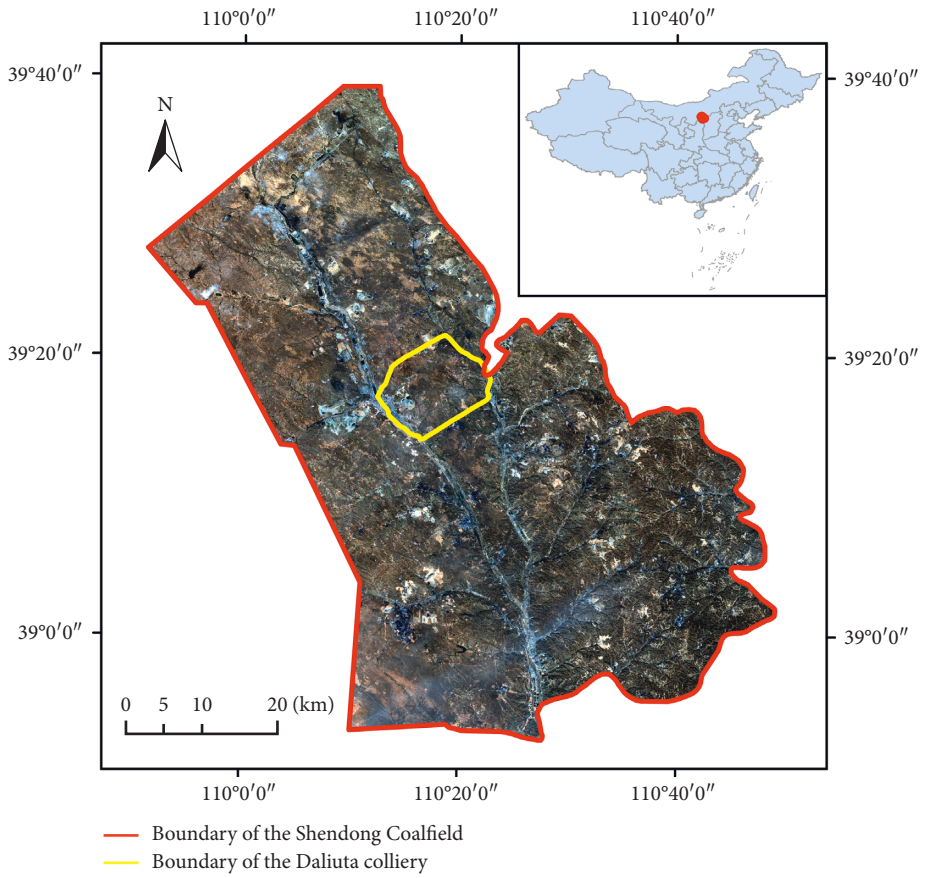

Figure 2: Location of the Shendong Coalfield.

3. Methods

In China, the most important method of studying dynamic mining subsidence characteristics is field monitoring, and the widely accepted mechanism are the section linear monitoring stations [21, 27, 34]. In July 2013, two surveying lines (i.e., line Z and Q) along the longitudinal and transverse direction were laid out above the SLWF. Line Z was located with 51 stations at 20 m intervals. While line Q was located with 35 stations at 25 m intervals (Figure 3). In addition, several stations at the end of lines Z and Q, regardless of those above the SLWF, were stable base stations that were located well outside the mining influence. According to the position of the working face and subsidence magnitude [21], four precise levelling was carried out using a Sokkia B20 optical level with a standard deviation of ± 5 mm for 1 km of double levelling, while the horizontal displacement was conducted via the Sokkia Set250X electronic total station.

It is notable that HUACE X93(1 + 1) GPS-RTK was employed to monitor the dynamic propagation and distribution ranges of surface cracks, particularly the development characteristics of surface cracks occurring above the SLWF. Additionally, the margin cracks which emerged around the edges of the subsidence trough were also measured [37].

4. Results and Analysis

4.1. Dynamic Surface Subsidence Characteristics. In Figures 4 and 5, each dynamic subsidence curve corresponds to the corresponding advance distance. Figure 4 shows the dynamic subsidence curves at different advance distances in the longitudinal direction. The initial subsidence trough shape appeared when the SLWF advanced 0.57 times the depth of mining (hereinafter referred to as "H"), and the subsidence trough margin on the side of the open-off cut presents a relatively steep shape, while there is a gentle slope on the side of the coal pillar. During the mining process after advanced 1.28 H, the trough margin on the side of the open-off cut was characterized by a steep shape with severe subsidence. And field monitoring indicated that there was severe discontinuous subsidence with many steps, where the largest drop of the steps is approximately 40 cm. However, the gentle trough margin above the coal pillars continuously developed as the SLWF advanced. Overall, the dynamic subsidence curve was asymmetrically characterized with a steep trough margin above the open-off cut, with a gentle one above the coal pillars. Moreover, the flat bottom of the subsidence trough already occurred when the SLWF advanced 1.63 H, indicating that the SLWF technique can accelerate the development process of subsidence troughs. It is notable that asymmetry also occurred in the dynamic

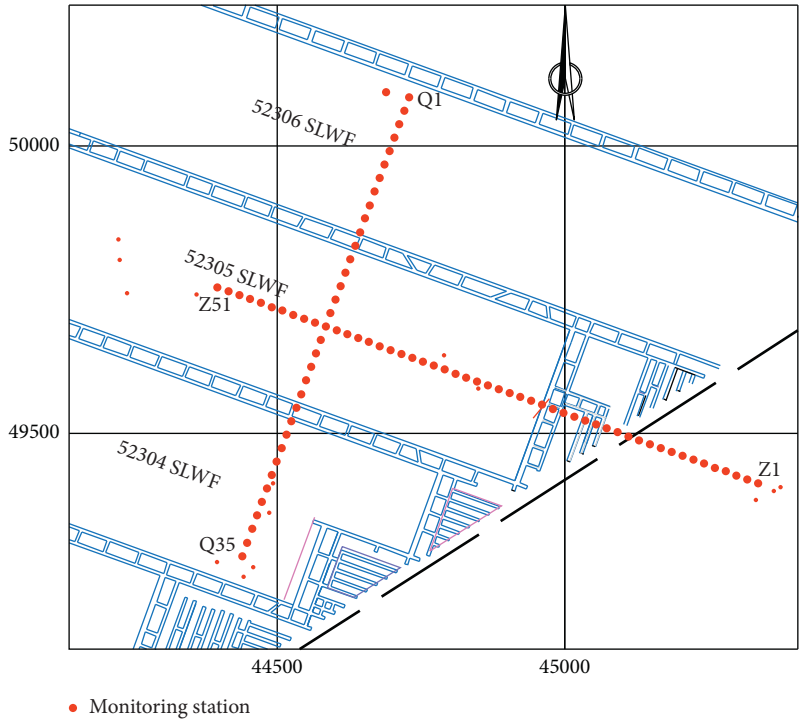

Figure 3: Layout of surface monitoring observations of 52305 SWLF.

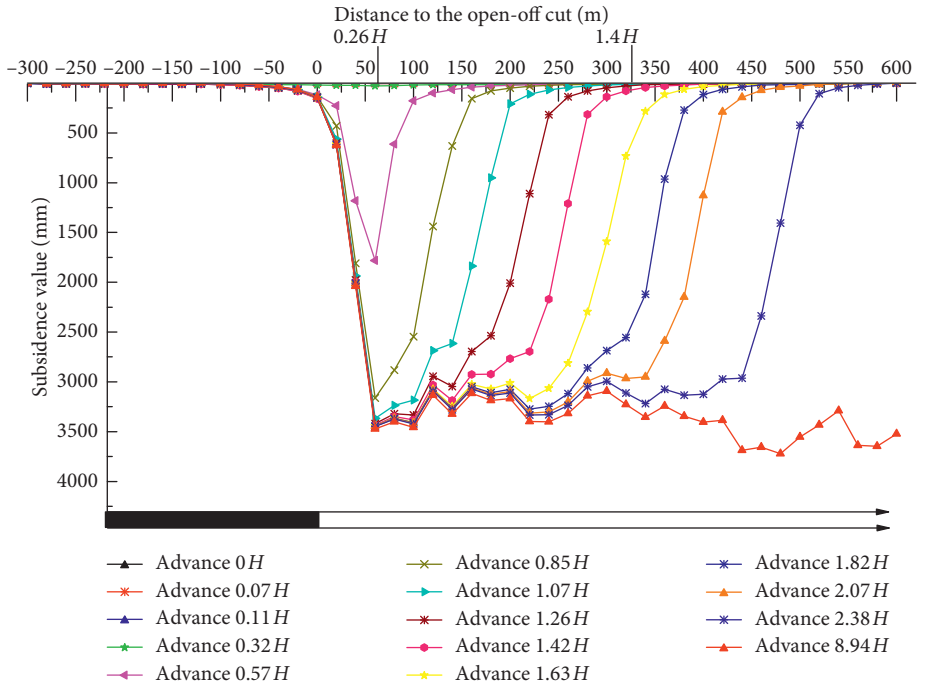

Figure 4: Dynamic subsidence curves of longitudinal line.

subsidence curve in the transverse direction (Figure 5). More precisely, the curve shapes on the side of adjacent old golf are more gradual than that on the side of the tailgate. Although the coal seam is approximately flat, the practice of 52305 SLWF resulted in the reactivation of "potential subsidence" of the adjacent old golf [9, 20, 21], which subsequently led to larger subsidence values and ranges above the goaf edge on the side of the tailgate (Figure 5), and the trough margin was characterized by a smaller slope and gentle shape.

4.2. Mining Subsidence Starting Distance. The advanced distance from the open-off cut to the position of the working face when the surface subsidence reaches 10 mm is

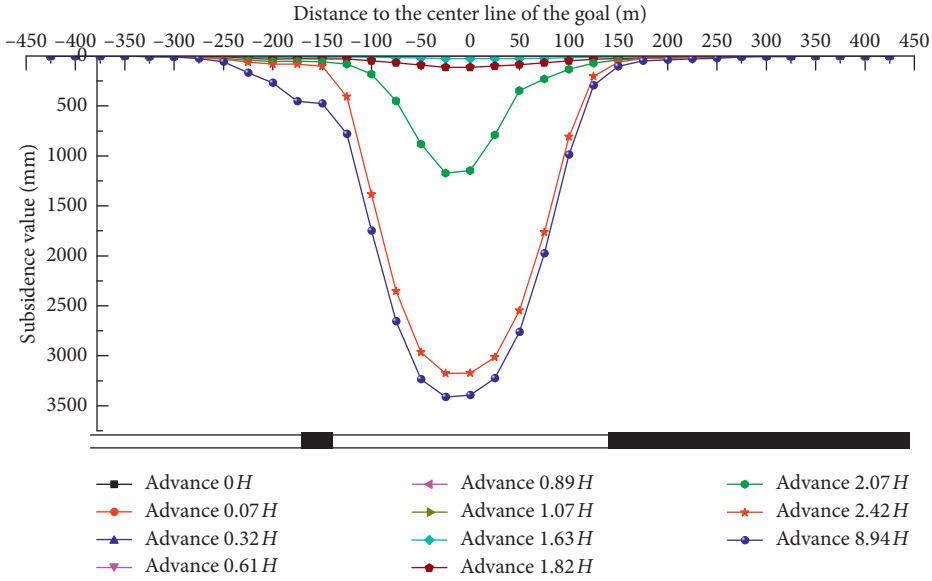

Figure 5: Dynamic subsidence curves of transverse line.

considered as the mining subsidence starting distance (the distance is generally distributed over the interval 1/4–1/2 H in China) [9, 21]. The starting distance reflected the initial advance distance influenced by underground mining, and it is mainly associated with H (i.e., the depth of mining), physicomechanical properties of overburden, and the presence of key stratum in the overburden.

The longer time interval between the second monitoring (advance 1/10 H) and third monitoring (advance 1/3 H) resulted in an insufficient monitoring density, which contributed to the actual starting distance not being measured in a timely manner. Hence, based on the field data, the average subsidence velocity of the Z24 station during the two monitoring times reached 2.3 mm/d (exceeding 1.67 mm/d), and the Z24 station was the point with maximum subsidence between the two monitoring times. Therefore, the Z24 station could most probably reach 10 mm of subsidence when the SLWF advanced 0.32 H; thus, the starting stance was smaller than 0.32 H. Furthermore, the relevant references indicate that the duration of dynamic subsidence is relatively short [29, 32]. Comprehensive analysis incorporating the advance speed and dynamic subsidence curves (longitudinal direction) via interpolation technique were conducted, and it could be logical inferred that the starting distance approached around 1/4 H, which was smaller than precious studies. And there are various factors such as the relative slow advance speed (4.1 m/d during the initial mining stage), larger average mining height of 6.7 m, the hard to medium rock, and the thick aeolian sand contributed to aforementioned phenomena.

4.3. Dynamic Characteristics and Analysis of Advance Influence Distance. It is widely accepted that the surface point where the subsidence initiated is always located at a fixed distance ahead of the instantaneous working face position. The fixed distance is defined as the advance influence distance (hereinafter referred to as"l"). The angle between the vertical line at the working face line and the line connecting the movement initiation point on the surface and the working face line is the angle of advance influence (hereinafter referred to as "w") [9]. The l and w are crucial parameters to determine the influence ranges of dynamic subsidence. However, the l, so called "a fixed distance," is actually a mean value in ideal conditions in relevant references [9, 20, 21], a constant l may not reflect the real dynamic mining process. Moreover, the field monitoring indicates that the l varies until the working face advanced a certain distance during the dynamic mining process (Figure 6), which differs from the precious studies [9, 20, 21].

Figure 6 shows that the l changes with the breaking of the rock strata during the mining process, especially when the significant ranges of variation occurred in the subcritical mining stage. However, there are still changes in l, but with small ranges of variation after the SLWF advanced 1.2 H. Overall, the dynamic curves of l accords with the exponential function characterized with one inflexion point and then approaches a constant. In addition, the average of five selected monitoring values of l is obtained when the SLWF advanced around 1.4 H; then the w is attained based on the following equation [21]:

$$w = \operatorname{arccot}\frac{l}{H}, \tag{1}$$

where w is the angle of advance influence, l is the advance influence distance, and H is the mining depth.

The calculated w is 69.7°, which is relatively large compared to the relevant references [28, 29], and there appears to be such factors as the advance speed, mining height, mechanical properties of the overburden rock, and critical mining, contributing to the determination of w. Some detailed analyses are performed, as follows:

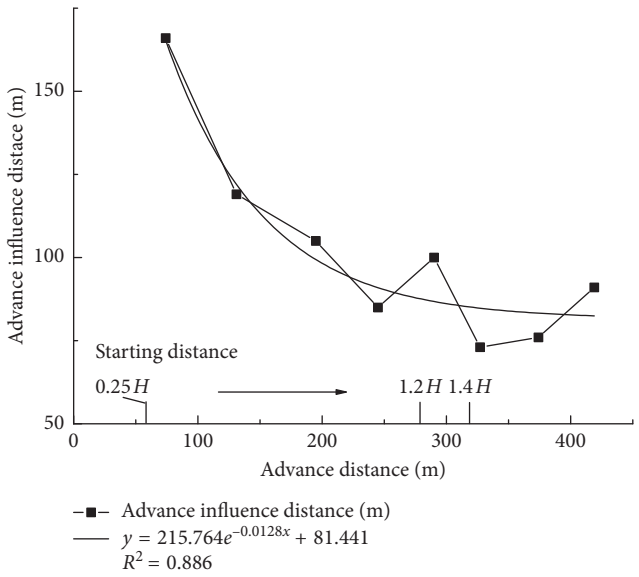

Figure 6: Dynamic curves of advance influence distance.

(1) The l increased progressively until the SLWF advanced around 1.2 H (Figure 6), where the SLWF transitioned from the subcritical state to the critical state. For instance, the l increased sharply to a peak after the SLWF advanced 0.25 H and then decreased, conforming to the exponential function (Figure 6), and it can be inferred that the failure and movement of the overburden stratum has a significant impact on the influence ranges of l, particularly the failure of key stratum can evidently lead to the variation of l, which is consistent with the literatures [25, 26, 38, 39]. And this can account for the average l, which should be obtained prior to the calculation of w [21, 23, 24, 29, 32, 33].

(2) The failure and subsidence of key stratum can result in the instantaneous surface subsidence. The presence of thin and hard bedrock makes the overburden rock vulnerable to failure. The rock movement and deformation can rapidly propagate to the surface layer of thick and loose aeolian sand. In addition, the aeolian sand is characterized by large fluidity and weak mechanical properties and structure, which is suitable for the rapid propagation of rock movement and deformation to the surface in the vertical direction [29]. Thus, the surface subsidence can reach 10 mm in a shorter time. Moreover, the highly intensive mining, characterized by large average advance speed (exceeding 12 m/d) and large mining height (6.7 m) after the SLWF advanced 1.2 H, resulted in the evolution characteristics of rock fissures being mainly of high angle and even vertical to the rock stratum and led to the reduction of advance influence range of overburden ahead of the coal pillars [40]. Therefore, the dynamic subsidence characteristics can reflect the failure and subsidence characteristics of overburden to some extent, contributing to a smaller l and a larger w inversely. Additionally, the weak plane due to the original soil fissures also resulted in the weak soil stratum and impeded the further propagation of movement and deformation horizontally, thus contributing to a smaller l.

(3) The variation of the advance speed can lead to the corresponding variation of rock breaking distance. Therefore, dynamic changes in surface subsidence emerge, which can account for variations in the l after the SLWF advanced 1.2 H.

4.4. Dynamic Characteristics and Analysis of Maximum Subsidence Rate

4.4.1. Maximum Surface Subsidence Rate. The subsidence rate, particularly, the maximum surface subsidence rate, may be the most visible parameter reflecting the magnitude of land damage and the movement intensity of the overburden stratum above the goaf, during the dynamic subsidence process [21, 27]. It is accepted that severe land ecology damage usually emerges where the maximum surface subsidence rate occurs. Based on field monitoring, the dynamic variations of the maximum surface subsidence rate in the longitudinal direction at different advance distances of the SLWF are shown in Figure 7.

The dynamic curve of maximum subsidence rate indicates that the maximum subsidence rate increased sharply with the SLWF continual advancing during the subcritical mining stage (before 1.2 H) (Figure 7), then the inflection point also occurred when the SLWF advanced 1.2 H, which may indicate that the SLWF undergoes the critical mining stage. Although there were still variations in the maximum surface subsidence rate with the SLWF advancing, the magnitude of variations is small. There are various factors acting on the maximum surface subsidence rate, such as the maximum subsidence, mining depth, mining height, mechanical properties of overburden, advance speed, and the magnitude of mining. The following empirical equation is for estimating the maximum surface subsidence rate [21, 24, 32]:

$$V_{\max} = \frac{KW_{\max}\overline{C}}{H}, \tag{2}$$

where K is the factor of subsidence rate, $\overline{C}$ is the average advance speed, H is the average mining depth, and $W_{\max}$is the maximum surface subsidence. In the present work, based on the field data, $\overline{C} = 12$ m/d, $H = 230$ m, $W_{\max} = 3722$ mm, and $V_{\max} = 617$ mm/d; thus, the K is 3.18, which is larger among the precious studies [30–33, 41].

It is notable that the variations of maximum surface subsidence rate can be attributed to the periodic failure of the key stratum which may sustain the overburden above the goaf [11], and the nonuniform advance rate in the critical mining stage may be responsible for the various amplitude of variations of the maximum subsidence rate [39, 42]. The notable inflection point occurred when the SLWF experienced from the subcritical mining to the critical mining,

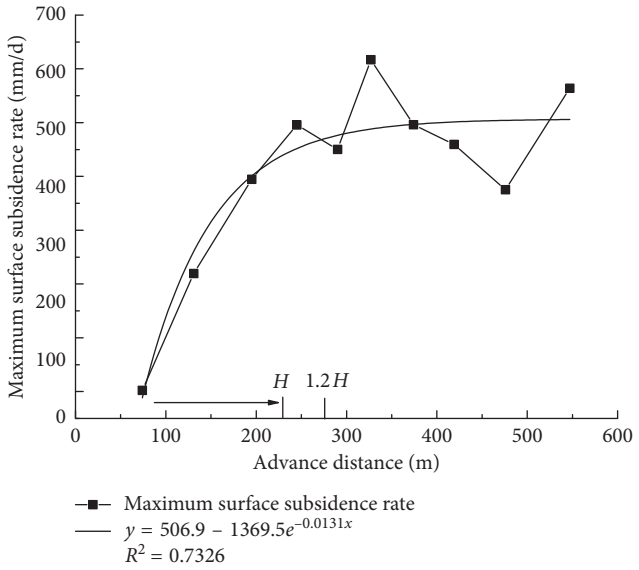

Figure 7: Dynamic curve of maximum subsidence rate.

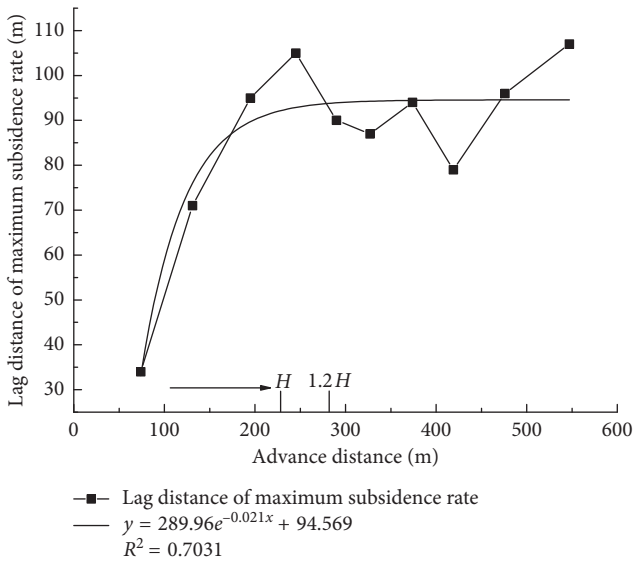

Figure 8: Dynamic curves of lag distance of maximum subsidence rate.

indicating that the critical mining may have posed a significant impact on the dynamic subsidence, particularly the maximum surface subsidence rate [25, 26, 38]. In addition, the larger plasticity of overburden comprising argillaceous cemented clastic rock series with a thickness of 0.57 H, shallow cover, and large advance speed are the major factors resulting in the larger K [32].

4.4.2. Lag Distance and Lag Angle of Maximum Subsidence Rate. It is well known that when the goaf reached the critical or supercritical dimension, the subsidence rate for each point on the major cross section in the longitudinal direction reached a maximum value under the prevailing conditions. The point where the maximum subsidence rate occurred lagged the corresponding position of the working face at a fixed distance (hereinafter referred to as "L") and remains so [9, 20, 21]. And the fixed distance is defined as the lag distance of the maximum subsidence rate. However, there are few studies on the L in the subcritical mining stage. In the present work, the relations between the L and the corresponding advance position of the working face are shown in Figure 8. It is notable that the L differed for each corresponding advance position. In addition, it increased sharply with the commencement of mining and reached an evident inflection point when the SLWF advanced around 1.2 H, then approached the steady state, and the dynamic curve of L also conformed to the exponential function.

Figure 8 shows that the overall variation trend of the lag distance is consistent with that of the maximum subsidence rate, which also indicated that the failure of key stratum and nonuniform advance rate may result in the previous phenomenon. And the critical mining can similarly have a considerable effect on the variation of L. When the SLWF reached the critical mining or steady state characterized with the periodic fracture of the key stratum, the average of several selected monitoring values of L was performed when the SLWF advanced around 1.4 H, and the $\overline{L}$ is ca. 94 m. Furthermore, the acute angle between the working face and the line connecting the point with the maximum subsidence rate is defined as the angle of the lag distance of maximum subsidence rate (hereinafter referred to as "Φ"), then the acute angle, 67.8°, can be attained based on the following empirical equation [9, 20, 21]:

$$\Phi = \operatorname{arccot}\frac{L}{H}, \tag{3}$$

where Φ is the angle of lag distance of maximum subsidence rate, L is the lag distance of the maximum subsidence rate, and H is the average mining depth.

A comparison between Φ in this work and those in the previous studies [28–30, 32, 33] indicates that the attained Φ is larger, which can be attributed to the prevailing conditions, such as the shallow cover, thin bedrock, large mining dimension, and rapid average advance speed (exceeding 12 m/d).Additionally, the poor mechanical structure of the thick aeolian sand, resulting in the rapid propagation of rock movement and deformation to the surface, is another reason responsible for the larger Φ. The evolution characteristics of Φ can be used to determine the most severe zones of dynamic subsidence, as well as the occurrence time and position of the maximum subsidence rate [9, 20, 21], which may be of benefit to the scientific monitoring of land ecology damage and the mining damage control.

4.4.3. Dynamic Subsidence Rate Curves of Surface Point with Maximum Subsidence Rate. It is widely accepted in China that the duration of surface subsidence could be divided into three stages according to the subsidence rate: the initial movement stage (which lasts from when a station commences subsidence to when the subsidence rate is larger than 1.67 mm/d), the active movement stage (during which the subsidence rate is larger than 1.67 mm/d), and the

attenuation stage (which lasts from when the subsidence rate is less than 1.67 mm/d to when the accumulated subsidence values do not exceed 30 mm in the successive six months) [21, 27]. Figure 4 shows that the maximum subsidence occurred at Z45 station. Unfortunately, being limited by insufficient monitoring density, it may not objectively reflect the actual duration of the dynamic subsidence process based on the field data of Z45 station, because it can homogenize the dynamic surface movement and deformation without characteristic points. Thus, the dynamic subsidence rate curve of Z33 station (Figure 9), where the maximum subsidence rate exceeding the other monitoring stations occurred, was taken as the research object to analyze the duration of dynamic subsidence; similar circumstances could be seen in literature [32].

Figure 9 shows that the Z33 station began to experience the initial movement stage when the position of working face was 0.79 H away to the Z33 station. Since the monitoring stations are sensitive to the mining disturbance due to the prevailing conditions, particularly the thick aeolian sand characterized with poor mechanical structure and strength, the subsidence rate of Z33 station increased rapidly to 1.67 mm/d when the position of the working face was 0.2 H away to the Z33 station and subsequently experienced the active movement stage. When the SLWF continually advanced and passed the Z33 station for a distance of 0.22 H, the acceleration of the subsidence rate reached 12.9 mm/day^2 and increased sharply to 184.8 mm/day^2 when the SLWF passed the Z33 station for a distance of 0.38 H, where the maximum subsidence rate of 617 mm/d occurred. Then, the subsidence rate decreased sharply, and the magnitude of subsidence rate were $0.36V_{\max}$, $0.07V_{\max}$, and $0.02V_{\max}$ when the working face passed the Z33 station for distances of 0.58 H, 0.78 H, and 1 H, respectively. The reduction magnitude of the subsidence rate was totally 98%. This indicated that severe surface movement and deformation occurred in the dynamic subsidence process, resulting in serious land ecology damage in various forms, such as severe stepped cracks [12, 36, 43–45], large variation of soil physical properties [12, 15, 17, 19], and damage to vegetation root due to ground strain [12, 46, 47]. Afterwards, there was an inflection point, ca. 1.2 H away to the position of the working face, which occurred in the dynamic curves of the maximum subsidence rate and the curves exhibited gently. The subsidence rate of Z33 station reached 1.67 mm/d when the working face passed it for a distance of ca. 6.42 H, indicating that the active movement stage terminated and the Z33 station commenced to experience the attenuation stage for a period of ca. 160 days. Thus, the ground approached stability, and the subsidence rate approximated zero.

As shown in Figure 9, active movement stage comprised of ca. 113 days, and the corresponding accumulated subsidence accounted for 98% of the total subsidence, whereas the duration of the severe stage comprised of merely 20 days (during which the average subsidence rate exceeds 10 mm/d), and the corresponding accumulated subsidence unexpectedly accounted for 95% of the total subsidence. Furthermore, such disasters as water-sand inrush, as well as the damage to vegetation roots due to ground strain, are vulnerable to happen. Thus, the severe stage is the key monitoring period of mining damage, deserving of more emphasis. However, the aforementioned phenomenon is mainly attributed to such factors as the highly intensive mining, rapid advance speed, poor mechanical structure, and high mechanical fluidity of the thick aeolian sand. Furthermore, the overburden rock and thick aeolian sand subsided instantaneously after the failure of key stratum. And the subsidence rate of each rock layer is faster and the relative suspending time is short, resulting in rapid propagation of rock movement to the surface characterized with severely concentrated and intense surface movement and deformation, larger surface maximum subsidence rate, and a shorter severe stage.

Additionally, the rapid advance speed was beneficial to the hinge joint of breaking hard rock blocks [44], forming a temporarily stable mechanical equilibrium structure [42]. And this may inhibit further severe migration of the breaking overburden and mitigate the subsidence of the overburden, contributing to a shorter severe stage, while there existed some space of separated key stratum, resulting in a longer attenuation stage due to the long-term mining-disturbed effect.

4.5. Dynamic Movement Trajectories of Surface Points. As is well known, the magnitude of the mining-disturbed effect on surface points varies with different relative positions between the surface points and the corresponding working face. Therefore, surface points above the goaf experienced a complex spatiotemporal process from the initial movement to severe subsidence, and finally to becoming steady [9, 21]. Since the SLWF dimension reached the supercritical size, the dynamic movement trajectories of the surface points at the major cross section conformed to the movement trajectories of the surface points due to supercritical mining [48] in the present work. Based on the distribution characteristic of the principal stress in rock and soil mass disturbed by mining [49], the sketch diagram of the dynamic movement trajectories of the surface points and the corresponding stress distribution in the rock and thick unconsolidated layer disturbed by mining was given, in a contrasting spatial view (Figure 10).

For instance, there are five surface points at the major cross section (Figure 10): points A and E were above the coal pillars, and points B, C, and D were above the goaf; particularly, point C was above the goaf center [48]. Points A and E were affected by mining, and their trajectories were basically towards the goaf center when the SLWF advanced from the point A′ to E′. Moreover, the trajectories of points B, C, and D were described as follows: as the face approached and went past a point, the cantilever strata below the point deflected progressively over the longitudinal rib, which was the source of horizontal movement and tensile stress. The movement was initially towards the reverse direction of the mining direction and finally towards the mining direction, while subsidence occurred throughout the whole dynamic process. The changing pattern of movement at a point can be explained in terms of

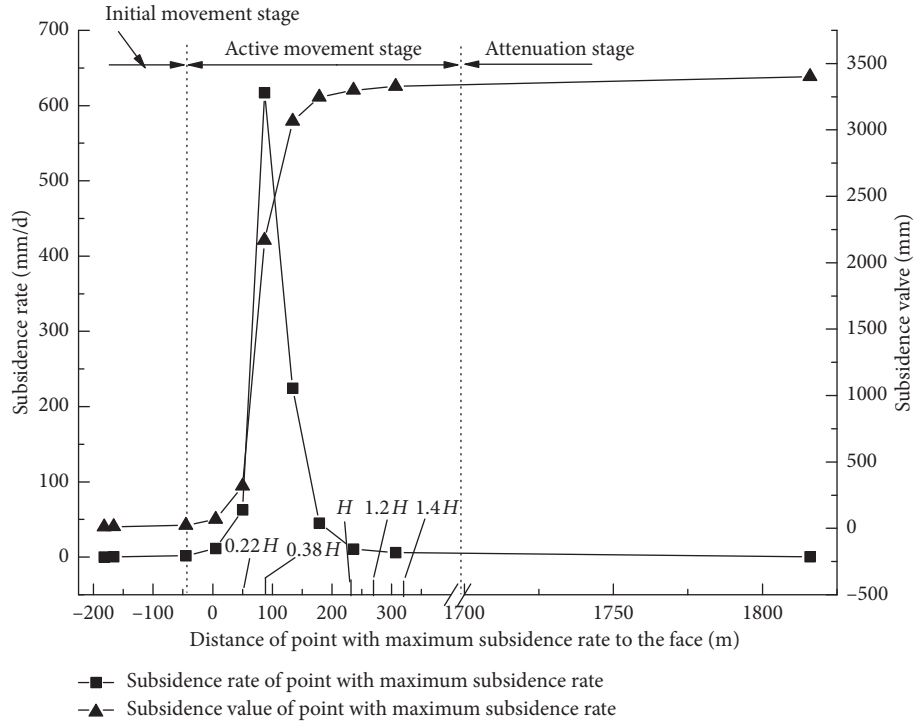

Figure 9: Dynamic subsidence rate curves of surface point with maximum subsidence rate.

the increase in cantilever bending and goafward rotation, and the movement of the strata at the point the working face approaches and gets under the point. Once the face goes past the point, the movements reverse in direction [50].

Figure 10 shows that there existed considerable differences in the dynamic trajectories of surface points. This can be attributed to various magnitudes of mining stress due to different positions of the surface points located above the goaf. Furthermore, compared to the traditional longwall mining, the ratio of the nondifferential subsidence area due to SLWF was larger [12]; therefore, there existed more points similar to point C above the goaf, which was affected by tensile stress after compressive stress. Therefore, the deformation could be recovered rapidly and approached the prior-mining state.

4.6. Dynamic Evolution and Distribution Characteristics of Surface Cracks. Many relevant references indicate that the surface cracks are the major form of land ecology damage due to mining [12, 14, 15, 17–19, 36, 46]. However, few attempts have been made concerning the dynamic distribution characteristics of surface cracks. Here, the HUACE X93(1 + 1) GPS-RTK was adopted to monitor the dynamic propagation and distribution ranges of surface cracks above the goaf (Figure 11). Furthermore, the margin cracks which appeared around the edges of the subsidence trough, as well as the attributive characters of surface cracks, were also measured [19, 37].

The filed data indicates that the distribution ranges of surface cracks due to SLWF continually expanded above the goaf. In brief, the overall distribution characteristics of surface cracks experienced three stages, including an elliptical shape, circular shape, and enlarged elliptical shape [19, 37]:

(1) *"Elliptical shape" stage*. Figure 11(a) shows that the surface cracks were disturbed in an elliptical shape and were symmetrical about the longitudinal line at the major cross section of the SLWF. Additionally, the length of the major axis and minor axis were 0.52 H and 0.29 H, respectively. The distributed range of surface cracks was 0.35 H–0.43 H away to the open-off cut. There existed evident discontinuous subsidence characterized with stepped cracks, the measured drop of the stepped crack is ca. 40 cm, while the width exceeds 15 cm. Thereafter, Figures 11(b)–11(d) show that the distribution ranges of surface cracks continuously expanded to the outside of the initial position, with the SLWF continuously advancing. Subsequently, the overall distribution characteristics of surface cracks transferred from the "elliptical shape" stage to the "circular shape" stage.

(2) *"Circular shape" stage*. Figure 11(c) shows that the surface cracks were distributed in a "circular shape" with a radius of around H when the working face advanced 1.12 H. Then, the distribution ranges of the surface cracks continuously expanded outward in a series of approximately concentric circles with the continuous advancing. Later, the marginal cracks propagated to the edges of the trough above the goaf when the SLWF advanced 1.37 H, while the maximum concentric circle radius is approximately 0.5 D_1 (i.e., the transverse length of the SLWF). Currently, it is worth noting that the crack angles on the side of

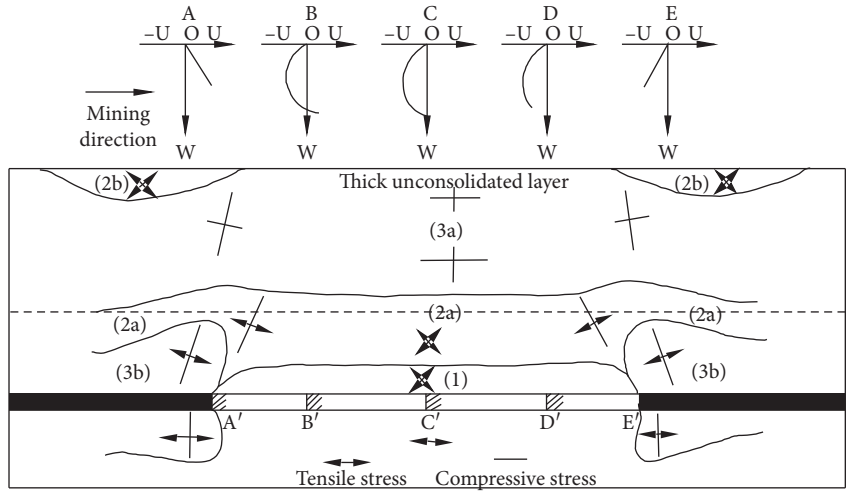

1 Tensile stress zone above goaf

2a Tensile–Compressive stress zone above goaf

2b Tensile–Compressive stress zone of top positive curvature region

3a Compressive stress zone of top negative curvature region

3b Supportive compressive zone

Figure 10: Dynamic trajectories of the surface points and the corresponding principal stress distribution in overburden disturbed by mining.

open-off cut, downhill, and uphill were 89.3°, 88.9°, and 88.5°, respectively, with an average of 88.9°, among which the surface cracks on the side of the open-off cut and uphill did not extend to the outside of the goaf, which indicated that the crack angles approached approximately the vertical angle, and the distribution ranges were restricted inside the edges of the goaf, resulting in relatively small ranges of land ecology damage [12, 23, 24], and moreover, the marginal cracks on the side of downhill expanded outside of the goaf, and the attributive characters including the drop of the stepped crack and the width are larger, which could be attributed to the uncrushed coal pillars between the adjacent working faces [22, 34] and stress concentration and discontinuous subsidence emerges in the overburden rock and soils due to the presence of coal pillars [22].

(3) *"Enlarged-elliptical shape" stage*. The margin cracks on the sides of the open-off cut, uphill, and downhill all expanded outside the edges of the goaf, but adjacent to the edges, and the corresponding crack angles are 89.4°, 87.7°, and 89.6°, respectively, with an average of 88.9°. Furthermore, compared with the previous stage, the changes of the crack angles was small, which indicated that little expanded ranges of land ecology damage occurred in the mining process [51]. The developmental characteristic of the surface cracks conformed to the "O shape" [52], and the evolutionary characteristics of surface cracks basically reflected the distribution characteristics of the overburden fissures in the mining process, providing the actual evidence for the theory of the "O shape" circle distribution of mining-induced fractures in the overlaying strata.

5. Discussion

Currently, the SLWF technology has been widely adopted in the Shendong Coalfield [10–12], and relevant reviews concerning with dynamic subsidence characteristics due to SLWF are summarized in Tables 1 and 2 [28–34, 41]. And there exist some particularities in the dynamic subsidence characteristics due to SLWF. Furthermore, it may be beneficial for the optimization of the prevailing monitoring strategy of land ecology damage, and worth further discussion. Additionally, the No. 1203 working face is the first fully mechanized coal mining working face in the Daliuta colliery [43], which can be referential for the present work. Thus, the relevant parameters of the No. 1203 working face together with the mining and geological data extracted from references [28–34, 41] are employed in this study. It is notable that the parameters such as D_1, D_3, h, Dip angle of coal seam, C, H, and h_1 indicate the mining and geological conditions. While other parameters such as p, j, V_{max}, $\tan\beta$, S_0, displacement angle, and crack angle indicate the movement and deformation magnitude. Particularly, the displacement angle and crack angle generally indicate the land damage ranges above the goaf.

5.1. Dynamic Formation Characteristics of Mining Subsidence Trough

(1) Tables 1 and 2 exhibit that more than 95% of the total subsidence occurred intensively during the active movement stage, of which the duration did not exceed 45% of the total subsidence duration, characterized with a relative large maximum surface subsidence rate [32]. And the subsidence trough can

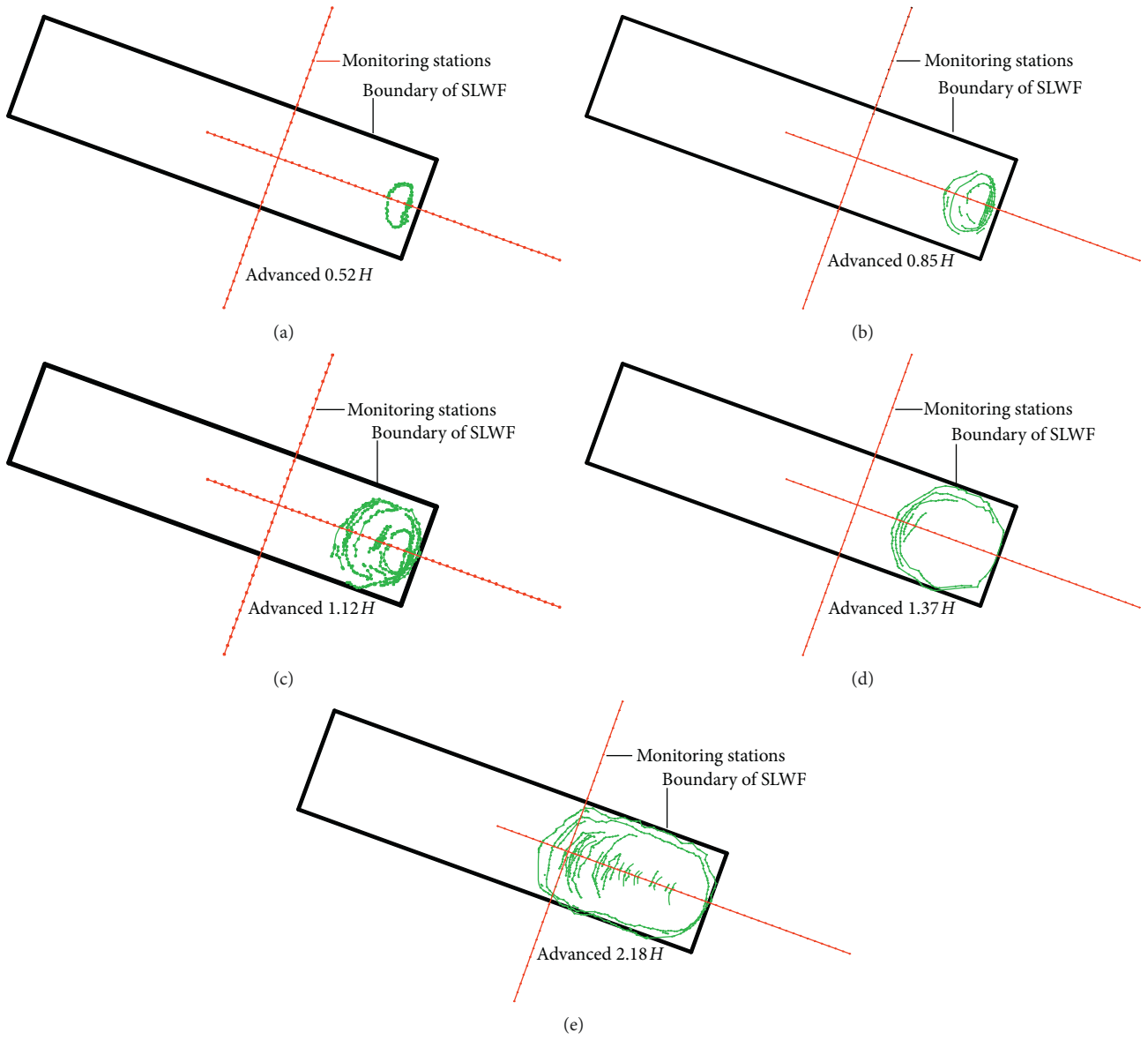

Figure 11: Dynamic extension and distribution of surface crack due to SLWF, (a) advanced 0.52 H; (b) advanced 0.85 H; (c) advanced 1.12 H; (d) advanced 1.37 H; (e) advanced 2.18 H [19, 37].

Table 1: Mining and geological conditions of some SLWF [28–34, 41].

Working face	D_1 (m)	D_3 (m)	h (m)	Dip angle of coal seam (°)	C (m/d)	H (m)	h_1 (m)
Daliuta colliery 1203	150.0	938.0	4.0	0.3	2.4	61.0	26.5
Daliuta colliery 52304	301.0	4547.6	6.5	1~3	9.0	225.0	30.0
Daliuta colliery 52305	280.5	2881.3	6.7	1~3	12.0	230.0	30.0
Buliuta colliery 12406	300.5	3592.0	4.5	1~3	12.0	200.0	16.9
Halagou colliery 22407	284.3	3224.1	5.2	1~3	15.0	130.0	15.7
Shangwan colliery 51101	240.0	4000.0	5.2	1~3	10.0	146.0	15.6
Buliuta colliery 31401	265.3	4629.0	4.2	1~3	13.5	255.0	/
Hanjiawan colliery 2304	268.0	1800.0	4.5	2~4	>10.0	135.0	/

rapidly form with a larger range of the flat bottom. For instance, the point 0.26 H away to the open-off cut above the 52305 SLWF reached its maximum subsidence rate when the SLWF advanced ca. 1.63 H. Moreover, the subsidence trough shape has basically formed, which could be owing to the following aspects. (i) Overlying rock stress changes do not fully propagate to distant regions due to the rapid advance

Table 2: Related surface subsidence parameters of some SLWF [28–34, 41].

Working face	p (%)	j (%)	V_{max} (mm/d)	tanβ	S_0 (m)	Displacement angle (°)	Crack angle (°)
Daliuta colliery 1203	65.0	97.0	131.8	2.6	20.4	69.7	75.3
Daliuta colliery 52304	41.2	98.0	430.0	2.9	37.5	82.0	—
Daliuta colliery 52305	40.0	98.0	617.0	2.7	39.5	83.3	88.1
Buliuta colliery 12406	—	96.0	268.0	2.5	40.0	82.5	88.5
Halagou colliery 22407	41.1	95.0	700.5	1.6	28.6	65.3	79.0
Shangwan colliery 51101	21.1	95.0	393.0	3.1	—	—	—
Buliuta colliery 31401	—	—	540.0	3.4	29.0	—	—
Hanjiawan colliery 2304	44.2	98.0	185.3	2.0	13.5	62.5	86~87°

Note. D_1 is the transverse length of SLWF, D_3 is the longitudinal length of SLWF, h is the average mining height, C is the advance speed, H is the average mining depth, h_1 is the average thickness of aeolian sand, V_{max} is the maximum subsidence rate, j represents the ratio of accumulated subsidence in the active movement stage accounting for the total subsidence, p represents the ratio of the duration of the active movement stage accounting for the total movement time, tanβ represents the tangent of major influence angle, S_0 is the offset distance of the inflection point, displacement angle is the acute angle between the line connecting the critical deformation value point and the goaf edge and the horizontal line on the side of coal pillar, and crack angle is the acute angle between the line connecting the outmost ground crack outside the subsidence trough and the goaf edge and the horizontal line on the side of coal pillar.

speed, and it failure to reach a new mechanical equilibrium state. The redistribution process of stress and displacement was insufficient, and the collapse of the overlying strata occurred due to the sudden instability of stress. This resulted in the rapid filling of the caving block into the goaf and the reduction of the overburden failure zone [53]. Thus, the corresponding differences between the maximum and minimum value of the rock stress could decrease, which is conducive to the postmining stability of mining-disturbed overlying rock. (ii) The overlying rock and the thick aeolian sand are characterized by the physicomechanical properties which can rapidly propagate movement and deformation, and then reach a steady state [29], since the goaf filled with caving block can rapidly approach a mechanical equilibrium state. Afterwards, the surface points would cease movement. (iii) The shear collapse of overlying rock resulted in rapid compaction of separated strata and the closure of mining-induced fractures [42], which contributed to the overburden reaching a mechanical equilibrium state after failure.

(2) The "enlarged-elliptical shape" [52] of the dynamic distribution characteristics of surface cracks during the mining process has been reported in relevant references [14, 19, 29, 33, 36]. The mining-induced marginal cracks usually appeared in "ribbon" and "O" shapes inside the edges of the SLWF. The distribution range of marginal cracks is small. Furthermore, Table 2 shows that the dynamic crack angles on the side of uphill and downhill approximated the vertical angle. The corresponding surface movement and deformation occurred intensively at the edges of the SLWF, and the severe discontinuous subsidence developed characterized with the steep edges of the subsidence trough and the stepped cracks, which were also reported in literatures [23, 24], concerning the mining area in eastern China. Overall, the stepped crack and the convergence of surface movement and deformation are the common features. However, with a more severe magnitude due to SLWF, the aforementioned phenomena might be attributed to such aspects as follows. (i) The overburden relative damage coefficient reduced [53] and the development and expansion of the rock fissures were inhibited owing to rapid advance and highly intensive mining [54]. Thus, the enrichment zone of the overlying rock fissures is mainly concentrated around the coal wall. Additionally, the main roof shear collapse along the roof control line was affected by the high support force [35, 53], resulting in the emergence of surface cracks perpendicular to the mining direction under the load of the overlying unconsolidated layers. Therefore, the rock fissures are mainly those approximately perpendicular to the rock stratum. (ii) The shear collapse of the overburden released the strain energy [30], and there existed a certain amount of weak vertical planes well developed in the thick aeolian sand due to its poor mechanical structure. The weak vertical planes can form weak plane of structure, which could expand rapidly and connect to each other due to mining. Then, the weak planes resulting from the original soil fissures contributed to the weak soil stratum, surface cracks appeared when the accumulated mining-induced stress exceeded the mechanical strength of the weak soil stratum at the weak plane. And the stress-strain released at the surface cracks, which may not only inhibit the further propagation of stress-strain, but may also impede the movement and deformation outside of the goaf. Finally, the movement and deformation occurred intensively at the edges above the goaf, leading to a larger crack angle and displacement angle, which was characterized by the convergence of movement and deformation, steep edges of the subsidence trough, and well-developed stepped cracks; (iii) Table 2 shows that there existed larger tangents of major influence angle and offset distance of the inflection point, which also contributed to the convergence of movement and deformation and steep edges of the subsidence trough, trending internally to the goaf with a smaller distributed range of surface cracks. Overall, compared

with the traditional working face, the overburden deformation could be restored rapidly, as well as the formation of the subsidence trough due to the SLWF, resulting in the decrease of the disturbance number and area due to mining. Thus, the ranges and magnitude of land ecology damage substantially reduced [14], and it can be concluded logically that the land ecology damage has the evident characteristics of "self-healing" due to SLWF.

5.2. Commonalities Analysis of Dynamic Parameters Evolution Characteristics during Mining. Figures 6–8 show that generalities exist in the evolution characteristics of the dynamic parameters, such as the advance influence distance, the angle of advance influence, maximum subsidence rate, and the lag distance of maximum subsidence rate, while there is an evident inflection point occurring at various exponential curves. Previous studies indicated that surface points on the major cross section would experience a critical or supercritical mining stage after the initial subcritical mining stage due to SLWF. The initial fracture of the roof, particularly the main roof occurred after the commencement of mining with the initial weighting, resulted in severe ground pressure and surface subsidence, thereby intensifying the complexity and changes of the surface subsidence. When the SLWF reached the supercritical dimension, the periodic failure of the main roof, particularly the key stratum, as well as the periodic weighting, resulted in the certain regularity of the dynamic surface subsidence. Afterwards, the aforementioned dynamic subsidence parameters approached a steady state, though the fluctuation of the parameters occurred, which has also been reported under the condition of thin alluvium [25] and thick unconsolidated layers [26]. Overall, the aforementioned phenomenon, considered as the generality, has been observed in different coal fields with various conditions. Therefore, this dynamic subsidence pattern appears to be owing to the forces associated with the mechanical changes and movement of the overburden failure, rather than attributed to any unique geological characteristics of the overburden in and around the study area. However, due to severe initial pressure and discontinuous subsidence, more emphasis should be placed on such aspects as follows: (i) In the process prior to the initial weighting and following it, the pressure of the mine surrounding rock changes rapidly, while the coal and rock dynamic disasters, such as the rib spalling, falling, and failure of pressure supports, are prone to occur, as well as water-sand inrush [28, 38, 43–45, 53, 55]. Therefore, it is evident that this stage is the key period of mine disaster monitoring, and more attention should be paid to the roof support and monitoring of the surrounding rock pressure, etc. (ii) Generally, the mining disturbance reached the surface, and such nonlinear mechanical hazards as sinkholes, collapse funnels, and stepped cracks, are also prone to occur above the open-off cut [34, 53], or around it. As such, more attention should be paid to the surface activities above the goaf preventing any risk, and the monitoring density should be intensified: in other words, the monitoring cycle should be shortened in the server stage, the surface movement monitoring are advised to be conducted once a day, in case of the leakage of characteristic points of dynamic subsidence and the critical development characteristics of surface cracks.

5.3. Optimized Strategy of Land Ecology Damages Monitoring. The evolution characteristics of dynamic subsidence parameters show that for a particular zone of land ecology damage above the goaf, the severe stage commenced from the initiation of the active movement stage to the closure of the dynamic cracks, during which the changes of subsidence rates occurred rapidly, including the maximum subsidence rate. Moreover, many relevant references show that the land ecology damage pattern appears to be the surface cracks [35–37, 53], in particular, the stepped cracks and subsidence, and the derived consequences, such as the changes of soil physicochemical properties and vegetation root damage due to stress-strain [12, 18, 46, 47], rather than the subsidence trough with seasonal or perennial waterlogging in eastern China [3, 4]. However, some samplings and observations at some spatiotemporal nodes are usually performed in the previous methods, the monitoring duration and sample area may not be scientific and accurate, and there appears to be some fuzziness and blindness. Consequently, the field results might fail to truly reflect the impact of underground coal mining on the land ecology. Therefore, from the perspective of targeted monitoring, the severe zone of land ecology damage located at the open-off cut to the inflection point of the curves of the dynamic subsidence parameters (Figure 12), and such key monitoring elements as soil physicochemical characteristics, vegetation root damage due to stress-strain, and the initial development pattern of surface cracks, occurred in this region. Thus, the sample points should be laid out reasonably and, more emphasis should be placed on the field monitoring in this region. As to the regions from the aforementioned inflection point to the position of the working face, large-scale and long-term field monitoring in previous studies appears to be time-consuming and laborious. A "ribbon" of dynamic cracks can be considered as the dynamic monitoring strip. Thereafter, the strip width may be determined according to the lag distance of maximum subsidence, incorporating the monitoring of dynamic subsidence, and in situ and dynamic monitoring of key monitoring elements can be performed logically. And the results may effectively reveal the impacts of SLWF on the land ecology, while reducing unnecessary manpower and time.

In addition, the stress intensity and spatial distribution of the soil deformation can be predicted based on field monitoring and mining subsidence theory [46, 47]. Afterwards, quantitative prediction of root damage of psammophilous vegetation due to SLWF can be attained, incorporating the mechanical strength characteristics of such psammophilous vegetation as Salix psammopbylla, Artemisia ordosica. Based on this, further optimization of SLWF would be carried out [8], which would play a

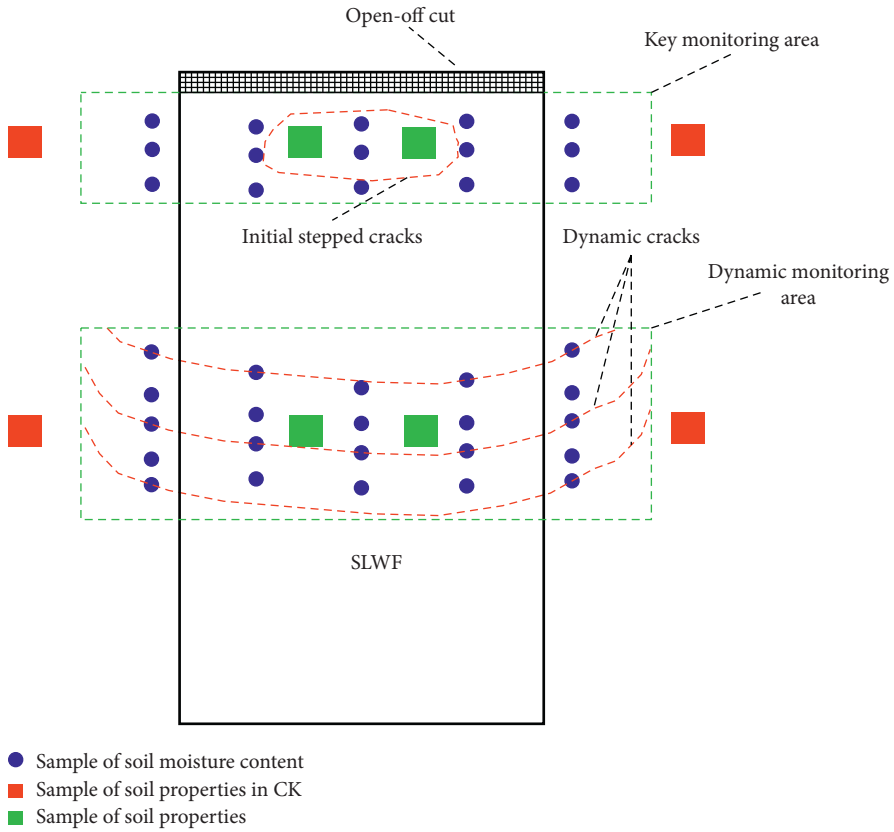

Figure 12: Optimized strategy of land ecology damages monitoring.

significant role in the development of mining technology characterized with active mitigation of ecology damage.

6. Conclusion

Adequate study on dynamic subsidence characteristics is the theoretical basis for mining damage control and land ecology monitoring. In this paper, the dynamic subsidence characteristics have been studied systematically, and the main conclusions in this paper are as follows.

(1) The observed surface maximum subsidence rate is 617 mm/d, and the subsidence trough can rapidly form. The subsidence trough due to SLWF is characterized with such aspects as a larger uniform-differential subsidence area, steep edges, high convergence of the surface movement, and deformation.

(2) The dynamic curves of such parameters as the advance influence distance, the angle of advance influence, maximum subsidence rate, and the lag distance of the maximum subsidence rate, conform to the exponential curves characterized with an evident inflection point, and critical mining may have a significant impact on this. More attention should be paid to the disasters monitoring and the roof support during the disaster-prone period.

(3) The previous monitoring methods of land ecology damage may be optimized based on the evolution characteristics of the dynamic subsidence parameters, the key monitoring area, and the in situ and dynamic monitoring strip should be laid out. The simple strategy proposed in this study may be an effective method for targeted monitoring land ecology damage and qualitatively predicting the root damage of vegetation.

(4) The proper assessment of the severe magnitude and spatial distribution for dynamic surface subsidence would be acquired based on the dynamic subsidence characteristics, contributing to scientific division of land damage ranges, and the assessment of the magnitude of the damage due to mining for the fragile-ecological mining areas in northwestern China.

Data Availability

The data used to support the findings of this study are available from the corresponding author upon request.

Conflicts of Interest

The authors declare that there are no conflicts of interest regarding the publication of this paper.

Acknowledgments

This work was supported by the National Natural Science Foundation of China (NSFC) and Shenhua Group

Corporation Ltd. jointly funded project (grant number U1361203) and National Natural Science Foundation of China under Grant 41801380. The authors are grateful for the help and support of Shenhua Group Corporation Ltd.

References

[1] A. M. Lechner, T. Baumgartl, P. Matthew, and V. Glenn, "The impact of underground longwall mining on prime agricultural land: a review and research agenda," *Land Degradation and Development*, vol. 27, no. 6, pp. 1650–1663, 2014.

[2] Z. Bian, X. Miao, S. Lei, S.-E. Chen, W. Wang, and S. Struthers, "The challenges of reusing mining and mineral-processing wastes," *Science*, vol. 337, no. 6095, pp. 702-703, 2012.

[3] Z. Hu, G. Yang, W. Xiao, J. Li, Y. Yang, and Y. Yu, "Farmland damage and its impact on the overlapped areas of cropland and coal resources in the eastern plains of China," *Resources, Conservation and Recycling*, vol. 86, pp. 1–8, 2014.

[4] Y. Gao, D. Liu, X. Zhang, and M. He, "Analysis and optimization of entry stability in underground longwall mining," *Sustainability*, vol. 9, no. 11, p. 2079, 2017.

[5] BP, "Statistical reviews of world energy," 2016, http://www.bp.com/statisticalreview.

[6] W. Zhang, D. S. Zhang, L. X. Wu, and H. Z. Wang, "On-site radon detection of mining-induced fractures from overlying strata to the surface: a case study of the Baoshan coal mine in China," *Energies*, vol. 7, no. 12, pp. 8483–8507, 2014.

[7] G. Q. Chen, M. J. Wang, Z. J. Liu, and W. F. Chi, "The biogeophysical effects of revegetation around mining areas: a case study of Dongsheng mining areas in inner Mongolia," *Sustainability*, vol. 9, no. 4, p. 628, 2017.

[8] Q. Sun, J. X. Zhang, Q. Zhang, and X. Zhao, "Analysis and prevention of geo-environmental hazards with high-Intensive coal mining: a case study in China's western eco-environment frangible area," *Energies*, vol. 10, no. 6, p. 786, 2017.

[9] S. S. Peng, *Longwall Mining*, West Virginia University, Morgantown, WV, USA, 2nd edition, 2006.

[10] D. Z. Gu, "Water resource and surface ecology protection technology of modern coal mining in China's energy "Golden Triangle"," *Engineering Science*, vol. 15, pp. 102–107, 2013.

[11] J. F. Ju and J. L. Xu, "Structural characteristics of key strata and strata behaviour of a fully mechanized longwall face with 7.0 m height chocks," *International Journal of Rock Mechanics and Mining Sciences*, vol. 58, pp. 46–54, 2013.

[12] Z. Q. Hu and C. Chen, "Impact of underground coal mining on land ecology and its restoration in windy and sandy region," *Journal of Mining Science and Technology*, vol. 1, pp. 120–130, 2016.

[13] Z. G. Wang, Y. L. Bi, B. Jiang et al., "Arbuscular mycorrhizal fungi enhance soil carbon sequestration in the coalfields, northwest China," *Scientific Reports*, vol. 6, no. 1, p. 34336, 2016.

[14] Z. Q. Hu, J. H. Long, and X. J. Wang, "Self-healing, natural restoration and artificial restoration of ecological environment for coal mining," *Journal of China Coal Society*, vol. 39, pp. 1751–1757, 2014.

[15] D. J. Yang, Z. F. Bian, and S. G. Lei, "Impact on soil physical qualities by the subsidence of coal mining: a case study in Western China," *Environmental Earth Sciences*, vol. 75, no. 8, pp. 1–14, 2016.

[16] S. L. Tao, J. Y. Fang, X. Zhao et al., "Rapid loss of lakes on the Mongolian plateau," *Proceedings of the National Academy of Sciences of the United States of America*, vol. 112, no. 7, pp. 2281–2286, 2015.

[17] P. L. Shi, Y. X. Zhang, Z. Q. Hu, K. Ma, H. Wang, and T. Y. Chai, "The response of soil bacterial communities to mining subsidence in the west China aeolian sand area," *Applied Soil Ecology*, vol. 121, pp. 1–10, 2017.

[18] Z. F. Bian, S. G. Lei, H. LIU, and K. Z. Deng, "The process and countermeasures for ecological damage and restoration in coal mining area with super-size mining face at aeolian sandy site," *Journal of Mining and Safety Engineering*, vol. 33, pp. 305–310, 2016.

[19] X. J. Wang, Z. Q. Hu, Q. F. Hu, and C. Chen, "Evolution and self-healing characteristic of land ecological environment due to super-large coalface mining in windy and sandy region," *Journal of China Coal Society*, vol. 40, pp. 2166–2172, 2015.

[20] H. Kratzsch, *Mining Subsidence Engineering*, Springer-Verlag, New York, NY, USA, 1983.

[21] G. Q. He, L. Yang, G. D. Ling, F. C. Jia, and D. Hong, *Mining Subsidence Engineering*, China University of Mining & Technology Press, Xuzhou, China, 1991.

[22] E. F. Salmi, M. Nazem, and M. Karakus, "The effect of rock mass gradual deterioration on the mechanism of post-mining subsidence over shallow abandoned coal mines," *International Journal of Rock Mechanics and Mining Sciences*, vol. 91, pp. 59–71, 2017.

[23] Z. X. Tan, Z. S. Wang, Y. J. Li, X. M. Sun, and K. Z. Deng, "Field research on ground subsidence rules of Intensive fully-mechanized mining by sublevel caving," *Journal of Mining and Safety Engineering*, vol. 25, pp. 59–62, 2008.

[24] W. B. Guo, C. F. Huang, and J. J. Chen, "The dynamic surface movement characteristics of fully mechanized caving mining under thick hydrous collapsed loess," *Journal of China Coal Society*, vol. 35, pp. 38–43, 2010.

[25] J. Tang, J. A. Wang, and L. Wang, "Dynamic laws and characteristics of surface movement induced by mining under thin alluvium," *Rock and Soil Mechanics*, vol. 35, pp. 2958–2968, 2014.

[26] G. S. Xu, D. H. Li, D. F. Hou, and Y. B. Zhang, "Measurement and prediction of the transient surface movement and deformation induced by mining under thick alluvium," *Rock and Soil Mechanics*, vol. 37, pp. 2056–2062, 2016.

[27] H. Teng, J. L. Xu, D. Y. Xuan, and B. . l. Wang, "Surface subsidence characteristics of grout injection into overburden: case study of Yuandian no. 2 coalmine, China," *Environmental Earth Sciences*, vol. 6, pp. 1–11, 2016.

[28] M. S. Yi, *Study and Application of Key Strata Theory in Shallow Seam of Shendong Mining Area*, China University of Mining & Technology, Xuzhou, China, 2008.

[29] S. Z. Du, *The Rule of the Overlying Strata Movement and Their Phytoremediation Technology after Large-Scale Underground Mining Operation in Shendong Coal Mine Area*, China University of Mining & Technology, Beijing, China, 2010.

[30] P. Wang, *Research on Rules of Mining Ground Movement and Deformation with Large Mining Height in Han Jia Wan Coal Mine*, Xi'an University of Science and Technology, Xi'an, China, 2012.

[31] X. J. Wang, *Monitoring, Evolution and Self-Healing Characteristics of Land Damage Due to High Tension Coal Mining in Windy and Sandy Area*, China University of Mining & Technology, Beijing, China, 2014.

[32] J. J. Chen, *Deformation Mechanism and its Characteristic of the Surface and Overburden Due to High-Intensity Coal Mining under Wind-Deposited Sand Zone*, Henan Polytechnic University, Jiaozuo, China, 2015.

[33] J. Wang, H. H. Zhao, and J. G. Liu, "Study on dynamic law of surface movement above working face of shallow—buried coal seam with thin bedrock," *Mining Safety and Environmental Protection*, vol. 43, pp. 21–25, 2016.

[34] Z. Q. Hu, C. Chen, W. Xiao, X. J. Wang, and M. J. Gao, "Surface movement and deformation characteristics due to high-intensive coal mining in the windy and sandy region," *International Journal of Coal Science and Technology*, vol. 3, pp. 339–348, 2016.

[35] X. Y. Yu and S. L. Huang, "Analyzing falling crack failure of overburden strata of shallow coal seam and its control method," *Coal Geology and Exploration*, vol. 34, pp. 18–21, 2006.

[36] Z. Q. Hu, X. J. Wang, and A. M. He, "Distribution characteristic and development rules of ground fissures due to coal mining in windy and sandy region," *Journal of China Coal Society*, vol. 39, pp. 11–18, 2014.

[37] C. Chen, Y. L. Zhao, T. T. He, and Y. L. Li, "Small-scale land destruction features caused by coal mining subsidence ground cracks in windy desert area," *Coal Engineering*, vol. 48, pp. 130–132, 2016.

[38] J. F. Ju and J. L. Xu, "Surface stepped subsidence related to top-coal caving longwall mining of extremely thick coal seam under shallow cover," *International Journal of Rock Mechanics and Mining Sciences*, vol. 78, pp. 27–35, 2015.

[39] J. F. Ju, J. L. Xu, and W. B. Zhu, "Longwall chock sudden closure incident below coal pillar of adjacent upper mined coal seam under shallow cover in the Shendong coalfield," *International Journal of Rock Mechanics and Mining Sciences*, vol. 77, pp. 192–201, 2015.

[40] Y. J. Zhang and F. M. Li, "Monitoring analysis of fissure development evolution and height of overburden failure of high tension fully-mechanized caving mining," *Chinese Journal of Rock Mechanics and Engineering*, vol. 30, pp. 2294–2301, 2011.

[41] S. S. Peng, H. M. Li, and Y. Zhou, *Ground Control for the Shendong and Jungar Coal Fields*, Science Press, Beijing, China, 2015.

[42] G. W. Fan, D. S. Zhang, and L. Q. Ma, "Overburden movement and fracture distribution induced by longwall mining of the shallow coal seam in the Shendong coalfield," *Journal of China University of Mining and Technology*, vol. 40, pp. 196–201, 2011.

[43] J. C. Zhang and B. H. Shen, "Coal mining under aquifers in China: a case study," *International Journal of Rock Mechanics and Mining Sciences*, vol. 41, pp. 629–639, 2004.

[44] D. S. Zhang, G. W. Fan, Y. D. Liu, and L. Q. Ma, "Field trials of aquifer protection in longwall mining of shallow coal seams in China," *International Journal of Rock Mechanics and Mining Sciences*, vol. 47, pp. 908–914, 2010.

[45] D. S. Zhang, G. W. Fan, L. Q. Ma, and X. F. Wang, "Aquifer protection during longwall mining of shallow coal seams: a case study in the Shendong coalfield of China," *International Journal of Coal Geology*, vol. 86, pp. 190–196, 2011.

[46] D. J. Pan, N. Zhang, Y. M. Zhao, and S. G. Lei, "Characteristics and mesoscopic mechanics of vegetation roots damage induced by mining in western mining area," *Journal of China Coal Society*, vol. 42, pp. 373–380, 2017.

[47] Y. L. Ding, S. G. Lei, Z. F. Bian, and C. L. Xie, "Distortion-resistant ability of tetraena mongolica root at the mining subsidence area," *Journal of China University of Mining and Technology*, vol. 42, pp. 970–974, 2013.

[48] Y. Q. Xu, *Coal Mining*, China University of Mining & Technology Press, Xuzhou, China, 2009.

[49] W. H. Sui, *Engineering Geological Study and Soil Mass Deformation during Subsidence*, China University of Mining & Technology Press, Xuzhou, China, 1999.

[50] L. Holla, "Ground movement due to longwall mining in high relief areas in New South Wales, Australia," *International Journal of Rock Mechanics and Mining Sciences*, vol. 34, no. 5, pp. 775–787, 1997.

[51] B. Ghabraie, G. Ren, X. Y. Zhang, and J. Smith, "Physical modelling of subsidence from sequential extraction of partially overlapping longwall panels and study of substrata movement characteristics," *International Journal of Coal Geology*, vol. 140, pp. 71–83, 2015.

[52] M. G. Qian and J. L. Xu, "Study on the "O-shape" circle distribution characteristics of mining-induced fractures in the overlaying strata," *Journal of China Coal Society*, vol. 23, pp. 20–23, 1998.

[53] C. Chen and Z. Q. Hu, "Research advances in formation mechanism of ground crack due to coal mining subsidence in China," *Journal of China Coal Society*, vol. 43, pp. 810–823, 2018.

[54] Y. W. Peng, Q. X. Qi, H. Y. Li, and Z. G. Deng, "Numerical simulation and analysis on influencing factors of fractured zone height of high-strength underground mining," *Journal of China Coal Society*, vol. 34, pp. 145–149, 2009.

[55] P. Huang, F. Ju, K. V. Jessu, M. Xiao, and S. Guo, "Optimization and practice of support working resistance in fully-mechanized top coal caving in shallow thick seam," *Energies*, vol. 10, no. 9, p. 1406, 2017.